Applied Clay Science 58 (2012) 25–33

Contents lists available at SciVerse ScienceDirect

Applied Clay Science

journal homepage: www.elsevier.com/locate/clay

Research paper

Adsorption of picloram herbicide on iron oxide pillared montmorillonite

Jose L. Marco-Brown [a], C. Martín Barbosa-Lema [a], Rosa M. Torres Sánchez [b], Roberto C. Mercader [c], María dos Santos Afonso [a,*]

[a] Departamento de Química Inorgánica, Analítica y Química Física e INQUIMAE, FCEN, UBA, Ciudad Universitaria, Pabellón II, C1428EHA, Buenos Aires, Argentina
[b] CETMIC (Centro de Tecnología en Minerales y Cerámica), Camino Centenario y 506, CC (49) (B1897ZCA) M. B. Gonnet, Argentina
[c] Departamento de Física, IFLP, Facultad de Ciencias Exactas, Universidad Nacional de La Plata, La Plata, Argentina

ARTICLE INFO

Article history:
Received 10 August 2010
Received in revised form 20 December 2011
Accepted 3 January 2012
Available online 8 February 2012

Keywords:
Montmorillonite
Picloram
Pillared clay
Herbicides

ABSTRACT

The adsorption of picloram on Fe Oxide Pillared Clays (PILC) as a possible basis for the development of adsorbent materials for the remediation of polluted environments was studied. To this end, after characterizing PILC obtained from raw clay from Wyoming, USA by XRD, elemental analysis, Mössbauer spectroscopy, DTA, TGA and N_2 adsorption (BET), the picloram adsorption was studied at constant pH and ionic strength after 48 h equilibration with an aqueous solution of PCM. PCM adsorbed samples were characterized by SEM, zeta-potential vs pH functions, FTIR and TGA-DTA and the adsorption was modellated using Langmuir and Freundlich models.

The results reveal that the surface area and interlayer space of PILC are bigger than those of raw montmorillonite. An analysis of the adsorption isotherms of picloram on the PILC showed that picloram adsorption increases with decreasing pH. The adsorption of PCM on PILC was 150 times higher than that found for raw montmorillonite under similar conditions. The zeta-potential vs pH functions shape and FTIR indicated that PCM coordinates the surface iron centers throughout pyridinic nitrogen atom forming inner-sphere complexes. The much greater PCM adsorption on PILC turns the process into an excellent candidate to be used for dosing or remediation of pesticides.

1. Introduction

Pesticides are widely used for control of broad-leaf weeds and other vegetation. The behavior of pesticides in soil is a large dynamic phenomenon. After application, they may pass into streams, rivers (Palma et al., 2004) and lakes or leach through soil with the possibility of contaminating subsurface waters (Zhang, et al., 2000). Soils can be considered, to a first approximation, as a combination of the minerals that compose them (Taubaso et al., 2004). Since clays are one of these components with higher chemical reactivity, the study of the pesticides adsorption may be used as models for the overall behavior. Among the clays used to understand the adsorption behavior of several herbicides, montmorillonite clay mineral stands out among them because of their, low cost, high specific surface area, (Bojemueller et al., 2001) and evidence of the intercalation of the pesticides in the clay mineral interlayer can be followed by modifications of the (001) reflection (Aydin et al., 2009; Bojemueller et al., 2001; Chen et al., 2009; Cornejo et al., 2008; Damonte et al., 2007; Hocine et al., 2004; Khoury et al., 2010; Lombardi, et al., 2006; Suciu and Capri, 2009; Torres Sánchez et al., 2011; among others.).

Picloram, 4-amino-3,5,6-trichloropyridine-2-carboxilic acid (PCM) is a systematic herbicide that is used to control unwanted woody plants, broadleaf and deeply rooted herbaceous weeds in cereals such as wheat, barley, sugarcane and oats (FAO, 2007; Palma, et al., 2004; Zhang, et al., 2000). PCM is the most persistent herbicide of the chlorobenzoic acid family. One year after its application 10–30% of the amount of the applied herbicide was detected in some crops in Canada (Meru et al., 1990).

The anionic character of PCM at the pH of most soils and water environments (pKa≈2.3) generates its very low adsorption on soil particles and extremely high soil mobility (Biggar et al., 1978; Celis et al., 2002; Cheung and Biggar, 1974; Osteryoung and Whittaker, 1980). However, in soils with different contents of organic matter and clay minerals a relation between PCM adsorption and organic matter content was found (Biggar et al., 1978; Farmer and Aochi, 1974; Grover, 1971; Hamaker et al.;, 1966). Adsorption of PCM by clay minerals had been observed in very acid systems (Biggar et al., 1978), but no adsorption had been determined at pH values higher than 3 (Celis et al., 2002; Grover, 1971). Nevertheless, adsorption studies of picloram on non-modified clay minerals have indicated a low adsorption up to pH 9 (Marco-Brown et al., 2008).

Among clay substances, pillared clays (PILC) are interesting materials to be used as catalysts and adsorbents, due to its multi-charged centers, large area, high interlayer space and thermal stability. PILC synthesized with oxide pillars of Cr, Zr, Al, Ti, and Fe have been previously

* Corresponding author. Fax: +54 11 4576 3343.
E-mail address: dosantos@qi.fcen.uba.ar (M. dos Santos Afonso).

0169-1317/$ – see front matter © 2012 Elsevier B.V. All rights reserved.
doi:10.1016/j.clay.2012.01.004

used in studies of adsorption of organic compounds (Cheknane et al., 2010; Tchieda et al., 2010; Zermane et al., 2010; Zuo et al., 2011; among others) as well as toxic metals such as As, Cd, Cr, Co, and Cu (Belkhadem et al., 2008; Bhattacharyya and Gupta, 2008; Cañizares et al., 1999; Heylen and Vansant, 1997).

This work aims at studying the PCM adsorption on iron oxide pillared montmorillonite, which could serve to develop adsorbent materials for the remediation of polluted environments and to design materials for controlled release of herbicides.

2. Materials and methods

2.1. Materials

PCM (inset in Fig. 1) was supplied by Sigma-Aldrich Co., purity 100%, solubility in water 430 ppm, $pK_a = 2.3$ (Pavlovic et al., 2005) and used as received. All other chemical reagents were provided by Merck PA and used without any further purification. Water was purified in a Milli-Q system from Millipore Inc.

Montmorillonite API # 26, Clay Mineral Spur Wyoming was provided by Ward's Natural Science Establishment, Inc., USA. This montmorillonite (labeled Mt) was manually milled in an agate mortar and sieved to a particle size of less than 125 μm. The main properties determined in a previous work (Marco-Brown et al., 2008) are: purity >98%, cation exchange capacity (CEC) 128 meq/100 g, isoelectric point ($IEP_{pH} = 3.2$), external surface area 27 m^2/g and total specific surface area 611 m^2/g (Michot and Villieras, 2006). The structural formula and isomorphic substitutions of Mt were determined from the chemical analysis following the method of Siguin et al. (1994).

2.2. Preparation of pillared clay

The pillaring solution with 1 M concentration of Fe(III) was prepared by dissolution of $Fe(NO_3)_3.9H_2O$ salt at room temperature with the slow addition and vigorous stirring of a 2 M solution of KOH, until reaching a ratio of $OH^-/Fe = 2$. The pH was controlled to attain a value lower than 1.8 by adding drops of 6 M HCl when necessary. Afterward, the solution was kept at room temperature for 4 h with continuous stirring for aging.

Furthermore, a deionized water dispersion of 1 wt.% of Mt was mixed with the pillaring solution with a Fe/Mt ratio of 60 mmol Fe/g Mt. The mixture was allowed to react, stirring at room temperature for 12 h. Later on, the solid was obtained by centrifugation and washed by successive re-dispersions in deionized water followed by centrifugation until conductivity value lower than 10 μS was attained. Further the product was air-dried, heated at 300 °C for 2 h and denoted as Fe-PMt.

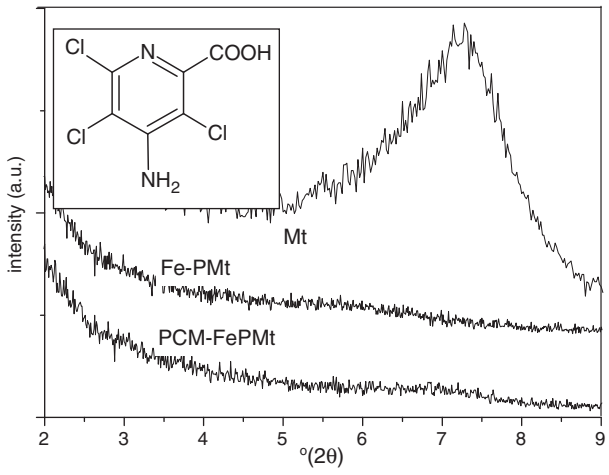

Fig. 1. XRD diffraction patterns of Mt, Fe-PMt and PCM-Mt.

2.3. Material characterizations

Composition of the Mt and Fe-PMt samples was determined by chemical analysis.

The specific surface area was determined by water adsorption at room temperature (S_w) (Torres Sánchez and Falasca, 1997) and nitrogen adsorption at 77 K (S_{N2}) on samples previously dried at 100 °C for 6 h at high vacuum using a Micromeritis AccuSorb 2100 E equipment internal or interlayer surface (S_I) was determined as the difference between total and external surfaces, S_w and S_{N2} respectively.

The X-ray diffraction patterns (reflection (001), counting time of 10 s/step collected from 3 to13° (2θ)) were obtained using a Philips 3020 with Cu Kα, 30 mA and 40 kV. Samples were X-rayed as semioriented at constant humidity (dispersion samples were dried maintaining a constant relative humidity (rh) of 0.47 for 48 h).

The electrophoretic mobility was determined in dispersions of Mt, Fe-PMt and Fe-PMt loaded with different amounts of PCM (PCM-FePMt) by microelectrophoresis in a Brookhaven equipment, using 10^{-3} M KCl as inert electrolyte. Samples were prepared at several pH values, and the content of total adsorbed PCM was measured.

The thermogravimetric measurements (TGA) were performed on 35 mg sample in a Shimadzu instrument (TGA-51H respectively), from room temperature to 800 °C at heating rate of 10 °C/min, in nitrogen atmosphere.

Scanning electron microscopy (SEM) was performed using a file emission gun scanning electron microscope Zeiss (FEG-SEM Zeiss LEO 982 GEMINI) with combined Energy Dispersive X-ray Analyzer (EDS), which provides the qualitative and semiquantitative composition of the samples. The SEM images were taken by applying 5 kV voltage with different magnification times for the clarification of surface. Mt, Fe-PMt and PCM-FePMt were fixed to 10 mm metal mounts using carbon tape and spit coated with gold under vacuum in an argon atmosphere. The surface morphology of the coated samples visualized by SEM permitted the identification of interesting structural features on the sample surfaces. INCA software was used to determine the elemental composition of the surface before and after solute binding.

Mössbauer spectra were taken in a conventional constant acceleration spectrometer of 512 channels with a 50 mCi nominal activity ^{57}CoRh source in transmission geometry. The absorbers were powder samples of about 105 mg cm^{-2} for both samples, calculated after the method described by Long et al. (1983), that yields the optimum absorber thickness. Isomer shifts were calibrated against an α-Fe foil at room temperature. Mössbauer spectra were analyzed with version 1.05 of the Recoil program (Lagarec and Rancourt, 1998).

Fourier-Transform Infrared Spectra (FTIR) of Fe-PMt, PCM and PCM-FePMt samples were recorded on FTIR Nicolet 8700 spectrometer using KBr discs in the 500–4000 cm^{-1} region. The PCM-FePMt sample was prepared at pH 5 by four successive adsorption processing using 10^{-3} M KCl solution as inert electrolyte, this accumulative adsorption process allowed to reach a surface coverage of Γ = 580 μmol/g.

2.4. Adsorption experiments

The clay mineral dispersion in deionized water (16 g clay/L) was previously adjusted at a determined value of pH of 3, 5 or 7 adding drops of concentrated HCl or KOH solution. After that, a determined PCM concentration, $C_{0,PCM,}$ was added to the clay mineral dispersion. All dispersions were prepared in 10^{-3} M KCl solutions, at temperature of T = 25 °C, with variable pH ranging between 3 and 7. The dispersion pHs were kept constant during the whole experiment.

The range of $C_{0,PCM}$ used in the adsorption isotherms was from 41 to 4970 for pH values of 5–7 and from 41 to 1657 μM for pH 3, respectively. The $C_{0,PCM}$ maximum concentration was established by the low solubility of PCM.

The solid samples were separated from the liquid phase by centrifugation at 17,000 rpm, stored in desiccators over silica gel, at room temperature for further analysis, and labeled PCM-Mt and PCM-FePMt, respectively. Control samples were prepared following the same procedure but without adding PCM.

The supernatants were filtered through 0.22 μm cellulose nitrate membrane and PCM concentration was determined by ion chromatography using a DIONEX DX-100 equipment, with a conductivity detector, a sample injection valve, and 25 μL sample loop. Two plastic anion columns, DIONEX AG-4 and AS-4, were coupled in series to serve as precolumn and analytical chromatographic column, respectively. A mixture of HCO_3^-/CO_3^{2-} of 4.25 mM/4.50 mM was chosen as eluent with a flow rate of 2 mL/min. The retention time of PCM under these experimental conditions was 3.2 min.

The amount of PCM adsorbed was determined as the difference between initial concentration and that of the supernatant in equilibrium. The solute concentration (C_{eq}) in the supernatant of Mt samples determined by ionic chromatography was higher than the initial one because a concentration effect of the adsorbate in the solution takes place due to the water volume adsorbed during the clay mineral swelling. After that, the PCM concentration at equilibrium was recalculated taking into account the adsorbed water determined by difference between dry clay mineral and solid samples.

All the isotherms were determined in duplicate. The typical experimental error was lower than 5% for all results.

3. Results and discussion

3.1. Sample characterization

Table 1 shows the clay mineral elemental composition, obtained by chemical analysis, expressed as oxides percentage.

The Mt sample structural formula obtained from chemical analysis was: $[(Si_{3.94}Al_{0.06})(Al_{1.56}Fe_{0.18}Mg_{0.26})O_{10}(OH)_2]M^+_{0.32}$. The Fe incorporated on Fe-PMt by pillaring method was evidenced by the increase of Fe_2O_3 percentage.

Table 2 shows the specific surface areas: total (S_w), external (S_{N2}) and internal ($S_I = S_w - S_{N2}$) (Michot and Villieras, 2006).

Specific surface for Mt and Fe-PMt samples determined by N_2 adsorption agrees with values obtained by Bojemueller et al. (2001) and Yuan et al. (2006), respectively. The S_w values increase from Mt to Fe-PMt samples, contrary to that found for Al-PILC (Yapar et al., 2009) indicating that the interlayer maintained a certain water adsorption capacity for the Fe-PMt sample.

The X-ray diffraction pattern (Fig. 1) of the Mt sample showed a (001) reflection at 1.42 nm (7.3°2θ). Pyrophyllite, a clay mineral that did not contain interlayer water has a (001) reflection at 0.92 nm (Erdemoglu et al., 2004). The differences between both (001) reflections suggest the predominance of several hydrated layers on Mt samples (Ferrage et al., 2005). Incorporation of Fe oxide in the montmorillonite interlayer resulted in the disappearance of the (001) reflection (Burch and Warburton, 1987; Chen et al., 1995). Yuan et al. (2008) found a d-spacing of 7.12 nm (1.2°2θ) for Fe-PILC, obtained with OH and Fe concentration in a ratio of $[OH^-]/[Fe^{+3}] = 2$. Some further work was done to investigate the structure of Fe-PILC, especially the specific formation mechanism of delaminated or pillared structure; Clinard et al. (2003) indicated that the 7.20 nm peak might be a reflection of a porous structure, rather than being attributed to simple intercalation.

Table 1
Oxide percentage determined by chemical analysis.

	Mt	Fe-PMt
SiO_2	65.82	35.03
Al_2O_3	23.08	12.58
Fe_2O_3	4.01	50.54
CaO	0.95	0.16
MgO	2.87	1.28
Na_2O	2.82	0.19
K_2O	0.46	0.22

Table 2
Specific surface areas: total (S_W), external (S_{N2},) and internal ($S_I = S_W - S_{N2}$).

Sample	S_W (m^2/g)	S_{N2} (m^2/g)	S_I (m^2/g)
Mt	632	27	611[a]
Fe-PMt	741	207	538

[a] Obtained from Marco-Brown et al. (2008).

3.2. Mössbauer

Fig. 2 displays the ^{57}Fe Mössbauer spectra of the two samples, Mt and Fe-PMt at room temperature. The spectra were measured in the range of velocities between −4 and +4 mm/s after no presence of any magnetically split signals in the spectra was investigated previously by taking spectra in the range of ±12 mm/s.

The spectra of both samples display two central doublets attributable to Fe^{3+} species. In the case of the original montmorillonite sample, Mt, in addition, two other signals can be fitted, that, according to Johnston and Cardile (1987), can be assigned to Fe^{3+} at tetrahedral sites and to Fe^{2+} ions located in trans-OH sites. In addition, there is also a component (not shown) that belongs to paramagnetic relaxation of electron spins in magnetically dilute systems (Murad, 1998). The Fe^{2+} signal is no longer noticed in the Fe-PMt sample spectra, indicating that all Fe ions in this sample are in a Fe^{3+} state. This oxidation was likely produced by the vigorous steps to which the original sample was subjected along the preparation method of the pillared clay.

Because of the substitution for Fe both in the oxygen tetrahedra and octahedra that lead to non-equivalent hyperfine sites for the Fe probes, the fittings were carried out using a program that takes into account the hyperfine field distributions using Voigt-shape lines (Lagarec and Rancourt, 1998). The parameters yielded by this procedure are shown in Table 3.

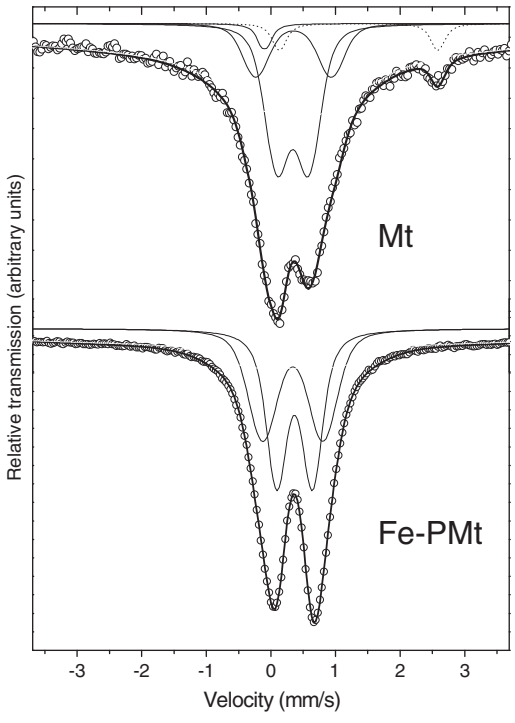

Fig. 2. Mössbauer spectra of Mt and Fe-PMt samples.

The intrinsic disordered nature of these phyllosilicates tends to render complex Mössbauer spectra, which in the literature have been correlated with other techniques, like X-ray diffraction, infrared and Raman spectroscopies or thermal analysis, to assign the different signals displayed in the spectra. In spite that in several cases it is possible to discriminate between *cis* and *trans* octahedral sites, in many others, X-ray diffraction studies have proved that there are discrepancies between the two techniques. These findings don't allow assigning unambiguously the origin of the signals making up the spectra (Murad and Wagner, 1994). Therefore, the parameters obtained from the fittings of such spectra are very dependent on the model used and should be considered only as a first order approach to the problem. The present case is not an exception and the assignments of the values reported in the table are just one of the many possibilities in which these spectra could be fitted. However, the assignment of the cis or trans sites of the OH at the oxygen octahedra in the samples is not the objective of the current study. Irrespectively of which model is used, there is a clear distinction between the original and the pillared montmorillonite.

The assignment used was that utilized by Johnston and Cardile (1987) for their montmorillonite sample from Drayton, Queensland, Australia, which displays three Fe^{3+} sites and one Fe^{2+} site. To consider the existing paramagnetic relaxations in dilute magnetic systems like the present phyllosilicates (that these authors have not taken into account) a highly distributed magnetic signal was added, which amounts to a significant area of the spectra.

3.3. Scanning electron microscopy

SEM image of Mt (Fig. 3A) showed face-to-edge contact between the particles with random orientation, and no formation of domains (group of particles which act as a unit) or clusters (group of domains which act as a unit) within the clay mineral bulk, while agglomerates were identified.

Yuan et al. (2006) indicate that the OH/Fe molar ratio of the initial pillaring solution has an important effect on the meso–microporous structure and the chemical composition of iron intercalated samples. These authors suggested that at high OH/Fe mole ratios of pillaring solutions, such as those used for Fe-PMt samples synthesis, some hydrated iron cations tend to aggregate, and the resulting large-sized iron aggregates remain outside the interlayer space and overlap the clay particles to form delaminated structures.

The modification of the clay mineral structure by the pillaring process is shown in Fig. 3B where pore spaces can be identified, and particles with sizes between 200 and 400 nm corresponding to co-aggregate or iron oxide particles on the surface of montmorillonite dispersed randomly in various directions can be observed. This structure modification remains without further changes after PCM adsorption (Fig. 3C). Elemental composition of the surface before and after adsorbate binding was determined by EDS. Iron content on external surface of Fe-PMt was drastically increased by the pillared process as is shown in Fig. 3. This increase of surface iron can lead to a substantial increase in the adsorption due to the changes on the identity and structure of the surface sites available for the adsorption.

Table 3
Room temperature Mössbauer parameters for samples Mt and Fe-PMt. Uncertainties are denoted as subindexes. Isomer shifts δ are referred to α-Fe at room temperature.

	$<\delta>$ (mm/s)	$<\lvert\Delta\rvert>$ (mm/s)	$<2\varepsilon>$ (mm/s)	$<\lvert H\rvert>$ (T)	Area (%)
Wyo					
QSD site 1	$0.34_{0.01}$	$0.49_{0.16}$			20_3
QSD site 2	$0.35_{0.01}$	$1.17_{0.25}$			8_2
QSD site 3	$-0.10_{0.01}$	$0.10_{0.06}$			$1.2_{1.0}$
QSD site 4	$1.36_{0.01}$	$2.45_{0.08}$			2.6_6
Mag. site 1	$0.38_{0.01}$		$0.00_{0.01}$	28_{21}	68_4
FeWyo					
QSD site 1	$0.37_{0.01}$	$0.56_{0.06}$			28_3
QSD site 2	$0.34_{0.03}$	$0.93_{0.30}$			26_4
Mag. site 1	$0.34_{0.03}$	$0.00_{0.01}$		28_{18}	46_3

3.4. Thermogravimetry analysis (TG-DTA)

Thermogravimetric (TG) and differential thermal analysis (DTA) are shown in Fig. 4. The weight-loss at 61 °C corresponds to desorption of the physically adsorbed water. Picloram melting point is t = 174 °C and the weight-loss due to PCM decomposition starts around the temperature of 200 °C (see inset figure in Fig. 4), then the sharp weight loss at around 355 °C of 2.1 wt.% for PCM-FePMt sample ($C_{0,PCM}$ = 400 ppm at pH = 3) can be assigned to the decomposition of PCM adsorbed (Fig. 4) indicating that this compound was retained at Fe-PMt structure above the PCM decomposition temperatures.

3.5. Adsorption isotherms

The PCM adsorption isotherms on Fe-PMt and Mt at pH 3, pH 5 and pH 7 are depicted in Fig. 5. The interactions of PCM with clay mineral surfaces, Mt and Fe-PMt, have an anionic profile, where adsorption decreases by pH increasing suggesting that the adsorption of PCM anion was coupled with a release of H_2O or OH^- ions, and being the adsorption favored by lower pH values.

The interaction of PCM with Fe-PMt surfaces takes place through the coordination of the pyridinic nitrogen atom to the metal center of the surface sites (see the PCM molecule structure depicted in the inset of Fig. 1). Similar results were found for picloram adsorption on Mt (Marco-Brown et al., 2008). Moreover, PCM can coordinate to free metals in aqueous solution such as Fe(III), Fe(II), Al(III), Cr(III), Cd(II), Zn(II) by forming dissolved complexes; where the pyridinic nitrogen atom is involved in the metal complexation (Bjelogrlić et al., 2010; Bombi et al., 2009; Calderazzo et al., 2003; González-Baró et al., 2008; among others).

Adsorption coverage (Γ_{ads}) of PCM on Fe-PMt was at least 150 times higher than on Mt. This adsorption increase can be ascribed to the surface site modifications by the pillared process with an iron content augment as was mentioned before.

Adsorption isotherms are important criteria in optimizing the use of adsorbents materials, because they describe the nature of the interaction between sorbate and adsorbent. Thus, analysis of experimentally obtained equilibrium data by either theoretical or empirical equations is useful for practical design and operation of adsorption systems.

There are a great number of expressions that describe adsorption isotherms; however, the most applied for the adsorption analyses on all types of materials are Langmuir and Freundlich models. Thus, experimental data for PCM adsorption were analyzed using both Langmuir and Freundlich models.

3.5.1. Langmuir adsorption isotherms

The Langmuir isotherm is a well known model that indicates a reduction of the available interaction places as the adsorbate concentration increases. The Langmuir isotherm assumes monolayer adsorption and is determined by the following equation:

$$\Gamma = \frac{\Gamma_{\max} * K_L * C_{eq}}{\left(1 + K_L * C_{eq}\right)} \quad (1)$$

where, Γ_{max} is the maximum uptake and means the maximum concentration on the solid phase, C_{eq} is the adsorbate concentration at the equilibrium on the aqueous media and K_L is the Langmuir equilibrium constant which is related with the free energy of the reaction.

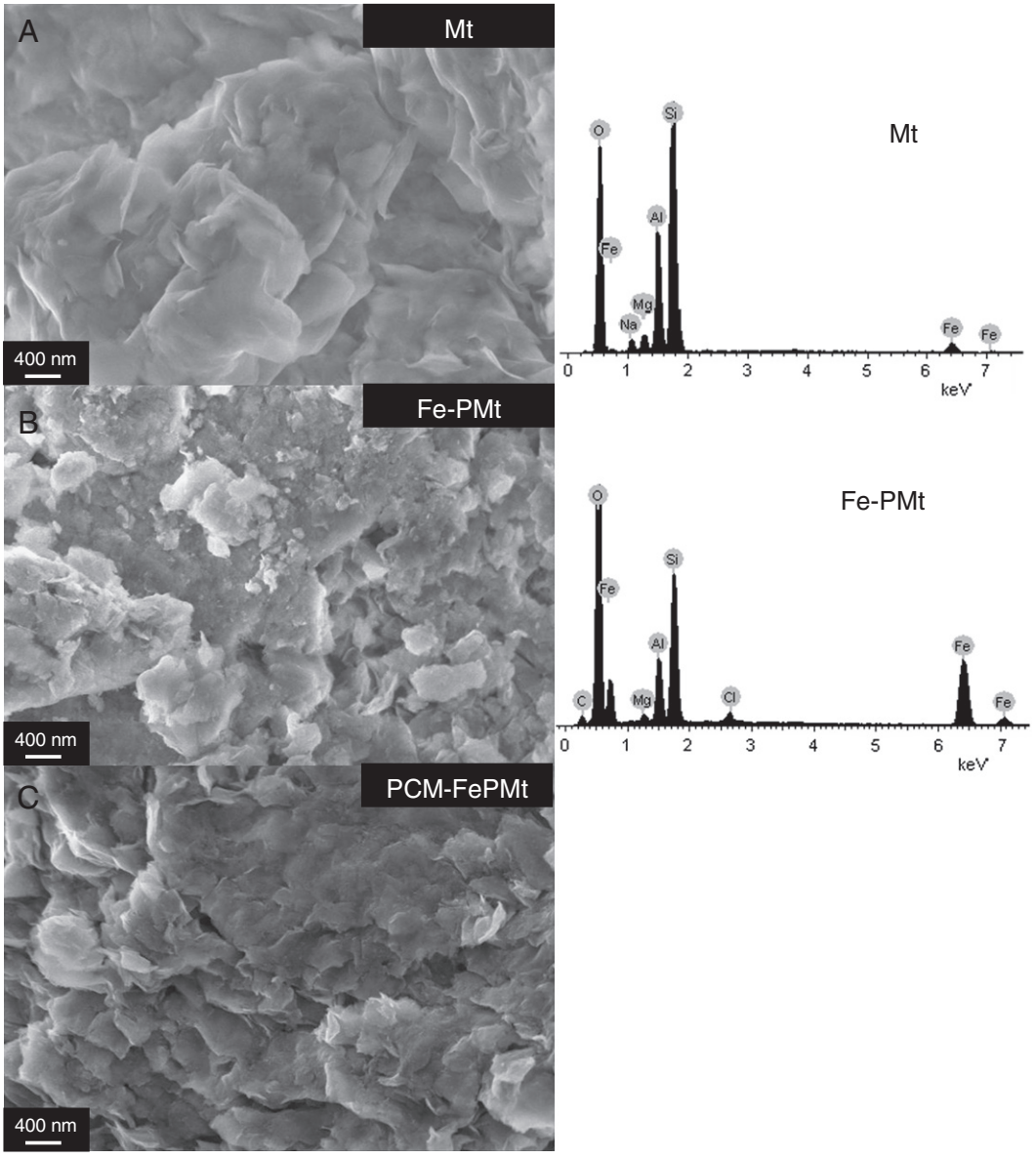

Fig. 3. EDX and SEM micrographies of (A) Mt, (B) Fe-PMt and (C) PCM-FePMt samples.

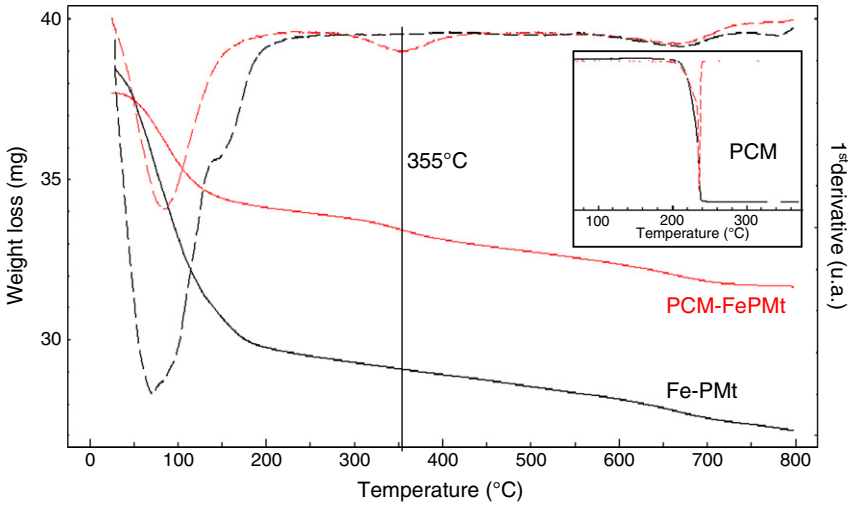

Fig. 4. TGA of Fe-PMt and PCM-FePMt. Dashed line correspond to the first derivative.

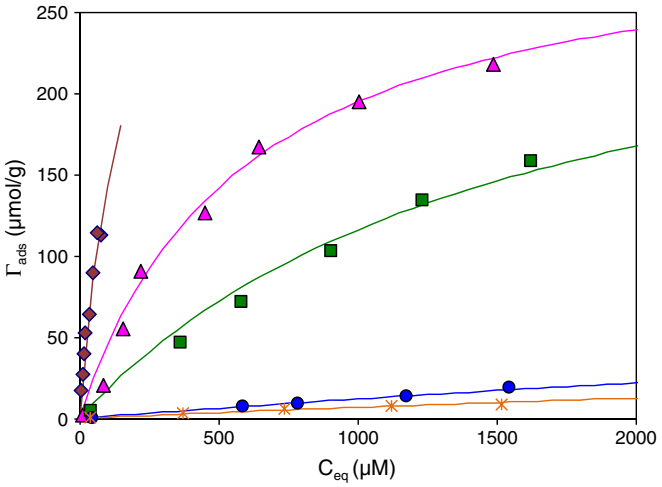

Fig. 5. PMC adsorption isotherms on Fe-PMt and Mt at different pHs. Symbols indicate: (♦) Fe-PMt pH = 3; (▲) Fe-PMt pH = 5; (■) Fe-PMt pH = 7.0; (●) Mt pH = 3.0 and (∗): Mt pH = 5.0. Solid lines were calculated using the Langmuir equation.

PCM adsorption isotherms for Fe-PMt are presented in Fig. 5. The Langmuir isotherm, Eq. (1), was applied to estimate the Fe-PICLs or clay mineral adsorption capacity. The Langmuir parameter and the correlation factor are indicated in Table 4. Affinity between sorbent and sorbate is represented by constant K_L. In general for good sorbents high Γ_{max} and high K_L are desirable.

The solid lines in Fig. 5 are the Langmuir model applied to PCM uptake during the adsorption process, and the calculated lines and the experimental data match very well with correlation coefficient (R^2) values between 0.9821 and 1.000.

3.5.2. Freundlich adsorption isotherms

The Freundlich isotherm is an empirical equation that describes the adsorption on a heterogeneous surface with a non-uniform distribution of heat of adsorption that means that the surface on which the adsorbed molecules are interactive is energetically heterogeneous. This model does not predict any saturation of the adsorbent by the sorbate. Instead, infinite surface coverage is predicted, indicating multilayer adsorption on the surface. This isotherm is represented by Eq. (2)

$$G_e = K_F * C_{eq}^{\,1/n} \quad (2)$$

where, K_F is the Freundlich constant indicating adsorption capacity and represents a measure of the surface area of the adsorbent while 1/n is an irrational fraction that varies between 0.1 and 1 and is a measure of the adsorption intensity.

Linear regression analysis was used for isotherm data treatment. The linear form of the Freundlich isotherm used was

$$\ln G_e = \ln K_F + (1/n) * \ln C_{eq}.$$

Table 4
Langmuir and Freundlich parameters for PCM adsorption onto Fe-PMt and Mt samples.

Sample	pH	Langmuir			Freundlich		
		K_L (L/mmol)	Γ_{max} (mmol/g)	R^2	K_F	n	R^2
Fe-PMt	3	6.00	0.38	0.9874	4.51	1.33	0.9784
	5	1.69	0.31	0.9932	3.75	1.76	0.9589
	7	0.63	0.30	0.9927	0.46	1.26	0.9973
Mt	3	0.092	0.14	1.0000	0.0140	1.02	0.9993
	5	0.089	0.08	0.9821	0.0226	1.21	0.9971

The values of K_F and 1/n were calculated from the intercept and slope of the plot between ln Γ_e vs ln C_{eq}. K_F, 1/n and the correlation coefficient (R^2) values of the Freundlich isotherm parameters were given in Table 4. These correlation coefficient (R^2) values are ranging between 0.9589 and 0.9993.

3.6. Fourier-Transform Infrared Spectra (FTIR)

FT-IR spectra of PCM, Fe-PMt and PCM-FePMt with a surface coverage of Γ = 580 μmol/g are shown in Fig. 6A and B. FT-IR spectra of PCM-FePMt reveal the presence of the herbicide adsorbed on the mineral surface through the presence of bands that correspond to PCM.

Two sharp bands appear in the high frequency area, 3474 and 3373 $cm^{-1,}$ of the spectrum of PCM corresponding to stretching vibrations of N – H. Around 3000 cm^{-1} is also present a broad band corresponding to νOH. Fe-PMt sample presents, in this frequency area, between 3600 and 3400 cm^{-1}, a broad band corresponding to the stretching vibration of the hydroxyl ions present on the mineral bulk or/and the intercalated water molecules. Due to the presence of this strong and broad absorption band of the stretching vibration of the hydroxyl ions, the shift of the stretching vibrations of N – H of PCM-FePMt sample cannot be observed.

The band at 1714 cm^{-1} in PCM corresponding to carboxyl C═O stretching shift to 1696 cm^{-1} of PCM-FePMt sample. This band had been associated with protonated carboxylic group indicating that some PCM is adsorbed as non-dissociated form (Celis et al., 2002).

The band at 1601 cm^{-1} corresponding to asymmetric stretching vibration ν_a of the dissociated carboxyl group and bending vibration of $-NH_2$ group of PCM is overlapping with the band at 1622 cm^{-1} of the mineral in PCM-FePMt.

The band at 1539 cm^{-1} present in both PCM and PCM-FePMt samples corresponds to pyridine-ring vibration ν(C═N). The doublet band at 1463 cm^{-1} of PCM appears like a single band at 1427 cm^{-1} of PCM-FePMt sample and it corresponds to pyridine-ring vibration ν(C═C).

The peak at 1380 cm^{-1} of PCM spectra corresponds to symmetric stretching vibration νs of the dissociated carboxyl group and it shifts to values of 1351 and 1363 cm^{-1} of PCM-FePMt sample. This shift could be attributed to the interaction of the PCM with the solid surface by the formation of a monodentate or bidentate coordination that involves the COO^- group and the nitrogen of the pyridine ring as was previously suggested by Loring et al. (2000) for picolinic acid interactions with Al(III)-(hydr)oxide minerals.

The shoulder at 1265 cm^{-1} of PCM-FePMt sample spectra corresponds to a shift of the PCM band centered at 1295 cm^{-1} and is due to pyridine δ(CH). The shoulder at 1239 cm^{-1} of PCM spectrum is observed in PCM-FePMt sample corresponding to NH deformation of the herbicide molecule. The shift of the wavenumber position of the CH out-of-plane deformation of PCM spectra from 991 cm^{-1} to 1014 cm^{-1} for PCM-FePMt sample indicates a coordination of PCM to mineral surface through the ring nitrogen in Loring et al. (2000). Similar results were reported for the adsorption of PCM on clay and Al(III), Fe(III) and Cu(III) saturated clays (Aochi and Farmer, 1981). These authors conclude that the interaction of PCM with mineral surfaces occurs through the nitrogen of the pyridine ring by the replacement of OH groups from the coordination sphere of copper. The interaction of PCM with Fe-PMt occurring throughout formation of a bridge complex between COO^- and nitrogen of the pyridine groups and iron(III) centers such as those previously suggested by Loring et al. (2000), and depicted in Fig. 7 is in agreement with inner sphere complexes formation.

3.7. Electrophoretic mobilities

The electrophoretic mobility is directly related to the zeta-potential and it is possible to calculate it using the Smoluchowski equation. The

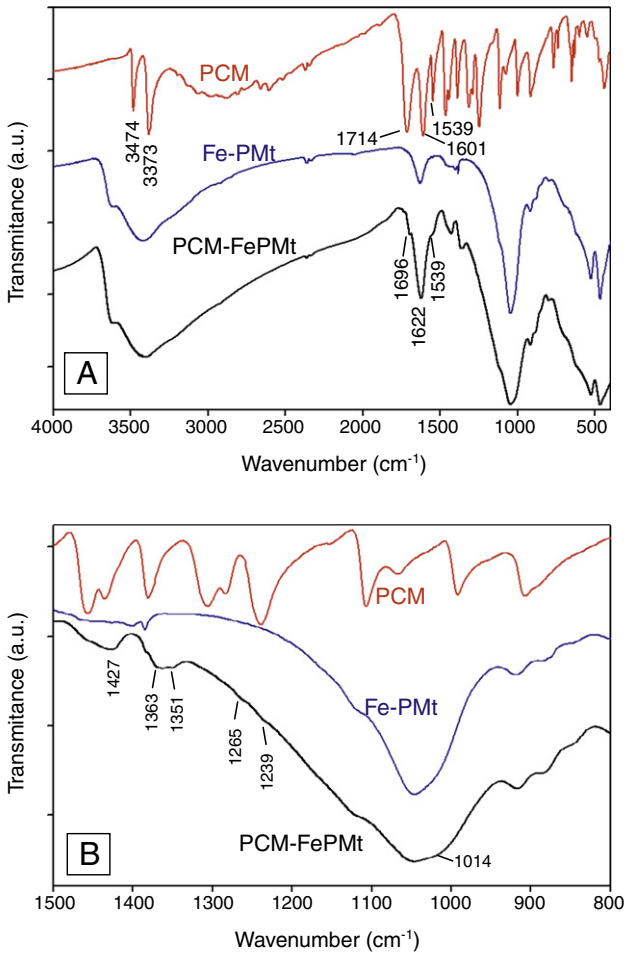

Fig. 6. FT-IR spectra of: (—) PCM, (—) Fe-PMt and (—) PCM-FePMt with a surface coverage of $\Gamma = 580$ μmol/g. A: Spectral region 400 to 4000 cm^{-1}. B: Spectral region 800 to 1500 cm^{-1}.

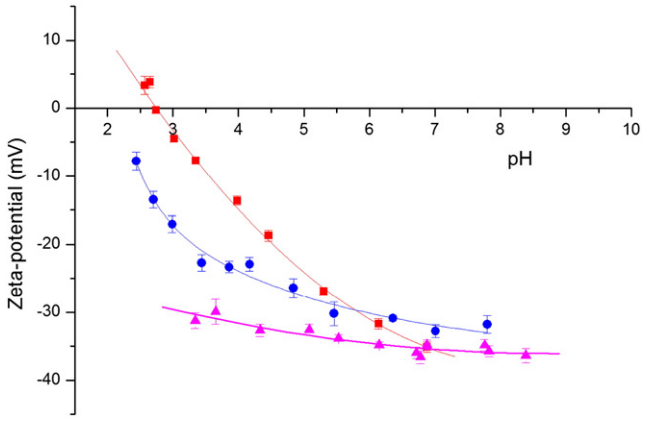

Fig. 8. Zeta-potential vs pH functions of (▲): Mt, (■): Fe-PMt and (●): PCM-FePMt with $\Gamma = 580$ μmol/g samples. All samples had an ionic strength $I = 10^{-3}$ M KCl.

zeta-potential functions for the Mt and Fe-PMt particles with and without adsorbed PCM at different pH values are shown in Fig. 8. This figure shows three zeta-potential vs pH functions: Mt, Fe-PMt and PCM-FePMt with a surface coverage of $\Gamma = 580$ μmol/g. The zeta-potential vs pH function of Mt sample was flat and did not show any significant change over a wide pH range, being around −35 mV in 1 mM KCl. This pH-independent zeta potential behavior is due to the layer structure of montmorillonite and it is associated to properties like high specific surface area and interlayer swelling and isomorphic substitutions of Si by Al in the montmorillonite structure that build a localized negative charge at the siloxane layer due to the differences on the oxidation state of those atoms. Although the overall particle charge is always negative, negatively and positively charged parts on the surface of clay minerals coexist simultaneously under acidic conditions (Tombácz and Szekeres, 2004).

It is also known that –OH groups are located on the edge sites, which corresponds only 1% of the total surface area (Lagaly et al., 2006) therefore, the pH-dependent edge groups did not affect the overall surface charge.

The iron incorporation on the clay mineral structure (Fe-PMt) changed the surface properties with incorporation of metallic centers of iron(III) as was previously shown by Tombácz et al. (2001) and was indicated by Mössbauer analysis. This iron(III) has a different acid–base behavior than sylanol and aluminol groups normally present on Mt surface. As a consequence of this the zeta-potential vs pH function has a different slope, similar to that for iron(III) (hydr)oxides (Tombácz et al., 2001). The PZC (point of zero charge) around pH 3 could be indicated. Thus, the change of the surface charge of Mt to more positive values in Fe-PMt was accounted for the modification of surface metal centers by the incorporation of iron (III) (Tombácz et al., 2001). This iron(III) atoms that are present at the Fe-PMt surface are coordinated to oxygen atoms and depending on the pH can become protonated ($\equiv FeOH_2^+$), neutral ($\equiv FeOH$) or deprotonated ($\equiv FeO^-$) at the surface of Fe-PMt samples by acid–base dissociation of the surface. Certainly, the total charge remains still negative at pH above 3 but the metallic centers of iron(III) are the new adsorption sites available on the surface that can be neutrally or positively charged at the working pH range.

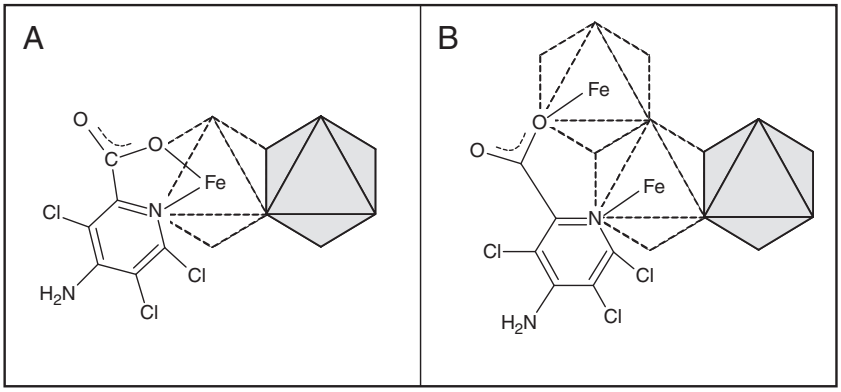

Fig. 7. Picloram surface complexes formed by coordination of COO^- and nitrogen of the pyridine groups with iron(III) centers represented by M. A: Bidentate complex. B: Bridge complex.

The IEP (isoelectric point) of PCM-FePMt sample shifted to lower pH values (extrapolation of zeta-potential vs pH function to 0 mV), respect to that found for Fe-PMt, due to PCM adsorption. The shift of IEP to lower values with PCM adsorbed indicates that the PCM adsorbs to the surface of the oxide as an anionic species as was mentioned before. Moreover, at constant and low pH values the leaving group is water and the incoming molecule is a negative group which leaves a residual negative charge on the surface and the zeta potential leads to more negative values. Also, at constant pH, the change of the surface charge is negative showing that the surface complexes formed are more negative than those formed during the surface protonation (Fig. 7A). Thus, PCM surface complexes contain a higher charge density than that of the protonated or deprotonated surface complexes formed during surface/water interaction.

As the pH increases the charge difference between Fe-PMT and PCM-FePMt samples is becoming smaller and the slope of the zeta potential vs pH function of PCM-FePMt sample becomes flat. This may be due to that the water leaving groups are now being replaced by hydroxyl group and the adsorbate exchange does not load changes on the charge, then the residual charge is lower than in the previous case.

At even higher pH, above 5.5, zeta potential function of PCM-FePMt sample is more positive than the zeta potential function of Fe-PMt sample. This is an indicative of the release of two hydroxyl groups followed by a bridge complex formation by coordination of N pyridine and the carboxylic group (Fig. 7B), then the residual charge is more positive. In this case, the surface complexes formed are less negative than those formed during the surface protonation.

As surface complexation takes place through the coordination of the pyridinic nitrogen atom to the metal center of the surface sites, also PCM carboxyl group could interact with hydroxylated sites or with clay mineral surface as was suspected previously by Celis et al. (2002) that studied picloram adsorption onto a number of clays exchanged with different inorganic and organic cations using FTIR.

Thus, these results provide indirect and conclusive evidence about the formation of surface complexes between the surface of the Fe-PMt particles and PCM and are in agreement with the results obtained from the FTIR spectra that suggested inner sphere complex formation.

This interaction could lead to steric shielding of the weakened hydroxyl groups or by protecting the surface sites and so prevent the surface deprotonation; or also reduce the number of active sites for the coordination of the surface by steric hindrance due to the size of the PCM anion.

4. Conclusions

The Fe-PMt sample was synthesized successfully, with a larger surface area than that obtained for Mt sample. XRD analysis showed that pillaring produces mainly a delamination of the raw clay mineral.

TGA analysis showed a strong interaction between PCM and Fe-PMt surface pointed out by the higher decomposition temperature of PCM-FePMt than Fe-PMt samples.

The Fe-PMt sample evidenced a higher adsorption capacity of picloram than that found for Mt sample. Interaction between PCM and Fe-PMt increased at acid pH values. The adsorption pH dependence indicated an anionic bonding mechanism of the PCM toward the Fe-PMt surface and FTIR spectra suggest inner sphere complex formation by coordination through pyridinic nitrogen atom and carboxyl group coordination.

PCM adsorption on a Fe-pillared montmorillonite is some orders higher than the adsorption on raw montmorillonite, and it demonstrates that Fe-PMt could serve to develop adsorbent materials for the remediation of polluted environments and to design materials for controlled release of herbicides.

Acknowledgments

The authors acknowledge Universidad de Buenos Aires, Secretaria de Ciencia y Técnica for financial support through Project UBACyT X043 and X067, Ministerio de Ciencia y Técnica, Agencia Nacional de Promoción Científica y Tecnológica, MINCyT-ANPCyT-FONCyT through PICT 23-32678 and Consejo Nacional de Investigaciones Científicas y Técnicas de la República Argentina (CONICET).

References

Aochi, Y., Farmer, W.J., 1981. Infrared spectroscopy of picloram interactions with Al(III)-, Fe(III)-, and Cu(III)-saturated and hydrous oxide-coated montmorillonite. Clays and Clay Minerals 29, 191–197.

Aydin, M.E., Ozcan, S., Beduk, F., 2009. Removal of lindane and dieldrin from aqueous solutions by montmorillonite and bentonite and optimization of parameters. Fresenius Environmental Bulletin 18, 911–916.

Belkhadem, F., Maldonado, A., Siebenhaar, B., Claces, J.M., Perez Zurita, M.J., Bengueddach, A., Figueras, F., 2008. Microcalorimetric measurement of the acid properties of pillared clays prepared by competitive cation exchange. Applied Clay Science 39, 28–37.

Bhattacharyya, K.G., Gupta, S.S., 2008. Adsorption of Fe(III), Co(II) and Ni(II) on ZrO-kaolinite and ZrO-montmorillonite surfaces in aqueous medium. Colloid Surface A 317 (1–3), 71–79.

Biggar, J., Mingelgrin, U., Cheung, M., 1978. Equilibrium and kinetics of adsorption of picloram and parathion with soils. Journal of Agricultural and Food Chemistry 26, 1306–1312.

Bjelogrlić, S., Todorović, T., Bacchi, A., Zec, M., Sladić, D., Srdić-Rajić, T., Radanović, D., Radulović, S., Pelizzi, G., Anđelković, K., 2010. Synthesis, structure and characterization of novel Cd(II) and Zn(II) complexes with the condensation product of 2-formylpyridine and selenosemicarbazide Antiproliferative activity of the synthesized complexes and related selenosemicarbazone complexes. Journal of Inorganic Biochemistry 104, 673–682.

Bojemueller, E., Nennemann, A., Lagaly, G., 2001. Enhanced pesticide adsorption by thermally modified bentonites. Applied Clay Science 18, 277–284.

Bombi, G.G., Aikebaier, R., Dean, A., Di Marco, V.B., Marton, D., Tapparo, A., 2009. Complexation of 2,6-pyridinedicarboxylic and 2,6-pyridinediacetic acids towards aluminium(III) and iron(III). Polyhedron 28, 327–335.

Burch, R., Warburton, C.I., 1987. Pillared clays as demetallisation catalysts. Applied Catalysis 33, 395–404.

Calderazzo, F., Englert, U., Hub, C., Marchetti, F., Pampaloni, G., Passarelli, V., Romano, A., Santi, R., 2003. Synthesis and structural characterization of iron(II) derivatives of heterocyclic tridentate amines. Inorganica Chimica Acta 344, 197–206.

Cañizares, P., Valverde, J.L., Sun Kou, M.R., Molina, C.B., 1999. Synthesis and characterization of PILCs with single and mixed oxide pillars prepared from two different bentonites. A comparative study. Microporous and Mesoporous Materials 29, 267–281.

Celis, R., Hermosín, M., Cornejo, L., Carrizosa, M., Cornejo, J., 2002. Clay–herbicide complexes to retard picloram leaching in soil. International Journal of Environmental and Analytical Chemistry 82, 503–517.

Cheknane, B., Baudu, M., Basly, J.-P., Bouras, O., 2010. Adsorption of basic dyes in single and mixture systems on granular inorganic–organic pillared clays. Environmental Technology 31 (7), 815–822.

Chen, J.P., Hausladen, M.C., Yang, R.T., 1995. Delaminated Fe_2O_3-pillared clay: its preparation, characterization, and activities for selective catalytic reduction of No by NH_3. Journal of Catalysis 151, 135–146.

Chen, H., He, X., Rong, X., Chen, W., Cai, P., Liang, W., Li, S., Huang, Q., 2009. Adsorption and biodegradation of carbaryl on montmorillonite, kaolinite and goethite. Applied Clay Science 46, 102–108.

Cheung, M., Biggar, J., 1974. Solubility and molecular structure of 4-amino-3,5,6-trichloropicolinic acid in relation to pH and temperature. Journal of Agricultural and Food Chemistry 22, 202–206.

Clinard, C., Mandalia, T., Tchoubar, D., Bergaya, F., 2003. HRTEM image filtration: nanostructural analysis of a pillared clay. Clays and Clay Minerals 51, 421–429.

Cornejo, J., Celis, R., Pavlovic, I., Ulibarri, M.A., 2008. Interactions of pesticides with clays and layered double hydroxides: a review. Clay Minerals 43, 155–175.

Damonte, M., Torres Sánchez, R.M., dos Santos Afonso, M., 2007. Some aspects of the glyphosate adsorption on montmorillonite and its calcined form. Applied Clay Science 36, 86–94.

Erdemoglu, M., Erdemoglu, S., Sayilkan, F., Akarsu, M., Sener, S., Sayilkan, H., 2004. Organo-functional modified pyrophyllite: preparation, characterization and Pb(II) ion adsorption property. Applied Clay Science 27, 41–52.

Farmer, W., Aochi, Y., 1974. Picloram sorption by soils. Soil Science Society of America—Proceedings 38, 418–423.

Ferrage, E., Tournassat, C., Lanson, B., 2005. Influence of the pH on the interlayer cationic composition and hydration state of Ca-Mont: analytical chemistry, chemical modeling and XRD profile modeling study. Geochimica et Cosmochimica Acta 69, 2797–2812.

Food and Agriculture Organization of the United Nations, 2007. FAO Specifications and Evaluations for Agricultural Pesticides. Picloram. http://www.fao.org.

González-Baró, A.C., Pis-Diez, R., Piro, O.E., Parajón-Costa, B.S., 2008. Crystal structures, theoretical calculations, spectroscopic and electrochemical properties of Cr(III) complexes with dipicolinic acid and 1,10-phenantroline. Polyhedron 27, 502–512.

Grover, R., 1971. Adsorption of picloram by soil colloids and various other adsorbents. Weed Science 19, 417–418.

Hamaker, J., Gorin, C., Youngson, C., 1966. Sorption of 4-amino-3,5,6-tricloropicolinic acid in soils. Adv. in Chem. Series, 60, pp. 23–27.
Heylen, I., Vansant, E.F., 1997. The difference in adsorption capacity between Fe-PILCs and modified Fe-BuA- and Fe-Zr-PILCs. Microporous Materials 10, 41–50.
Hocine, O., Boufatit, M., Khouider, A., 2004. Use of montmorillonite clays as adsorbents of hazardous pollutants. Desalination 167, 141–145.
Johnston, J.H., Cardile, C.M., 1987. Iron substitution in montmorillonite, illite, and glauconite by ^{57}Fe Mössbauer spectroscopy. Clays and Clay Minerals 35, 170–176.
Khoury, G.A., Gehris, T.C., Tribe, L., Torres Sánchez, R.M., dos Santos Afonso, M., 2010. Glyphosate adsorption on montmorillonite: an experimental and theoretical study of surface complexes. Applied Clay Science 50, 167–175.
Lagaly, G., Ogawa, M., Dékány, I., 2006. Clay mineral organic interactions. In: Bergaya, F., Theng, B.K.G., Lagaly, G. (Eds.), Handbook of Clay Sci. Elsevier, Amsterdam; London, pp. 309–378.
Lagarec, K., Rancourt, D.G., 1998. Mössbauer Spectral Analysis Software, Version 1.0. Department of Physics, University of Ottawa. Version 1.0.
Lombardi, B., Torres Sánchez, R., Eloy, P., Genet, M., 2006. Interaction of thiabendazole and benzimidazole with montmorillonite. Applied Clay Science 33, 59–65.
Long, G.J., Cranshaw, T.E., Longworth, G., 1983. The ideal Mössbauer effect absorber thickness. Mössbauer Effect Reference and Data Journal 6, 42–49.
Loring, J.S., Karlsson, M., Fawcett, W.R., Casey, Y., W. H.,, 2000. Attenuated total reflection-Fourier-transform infrared and ^{27}Al-nuclear magnetic resonance investigation of speciation and complexation in aqueous Al(III)-picolinate solutions. Geochimica et Cosmochimica Acta 64, 4115–4129.
Marco-Brown, J. L.; Barbosa, C. M.; Torres Sánchez, R. M., dos Santos Afonso, M., 2008. Movilidad y control del herbicida picloram en arcillas in Las Fronteras de la Física y Química Ambiental en Ibero América, 496–502, Ed. UNSAM, Buenos Aires, Argentina.
Meru, S., Liber, K., Stonefield, K., Solomon, K., Stephenson, G., 1990. Persistence and lateral movement of 2,4-dichlorophenoxy acetic acid and picloram on power line rights-of-way. Archives of Environmental Contamination and Toxicology 19, 572–577.
Michot, L.J., Villieras, F., 2006. Surface area and porosity. In: Bergaya, F., Theng, B.K., 680 Lagaly, G. (Eds.), Handbook of Clay Sci. Developments in Clay Sci., 1. Elsevier, 681 Amsterdam, pp. 965–978.
Murad, E., 1998. Clays and clay minerals: what can Mössbauer spectroscopy do to help understand them? Hyperfine Interactions 117, 39–70.
Murad, E., Wagner, U., 1994. The Mössbauer spectrum of illite. Clay Minerals 29, 1–10.
Osteryoung, J., Whittaker, J., 1980. Picloram: solubility and acid–base equilibria determined by normal pulse polarography. Journal of Agricultural and Food Chemistry 28, 95–97.
Palma, G., Sánchez, A., Olave, Y., Encina, F., Palma, R., Barra, R., 2004. Pesticide levels in surface waters in an agricultural-forestry basin in Southern Chile. Chemosphere 57, 763–770.
Pavlovic, I., Barriga, C., Hermosín, M., Cornejo, J., Ulibarri, M., 2005. Adsorption of acidic pesticides 2,4-D, clopyralid and picloram on calcined hydrocalcite. Applied Clay Science 30, 125–133.
Siguin, D., Ferreira, S., Froufe, L., García, F., 1994. Smectites, the relationship between their properties and isomorphic substitution. Journal of Materials Science 29, 4379–4384.
Suciu, N.A., Capri, E., 2009. Adsorption of chlorpyrifos, penconazole and metalaxyl from aqueous solution by modified clays. J. Environ. Sci. Health, Part. B: Pestic., Food Contam., Agric Wastes 44, 525–532.
Taubaso, C., dos Santos Afonso, M., Torres Sánchez, R.M., 2004. Modelling soil surface charge density using mineral composition. Geoderma 121, 123–133.
Tchieda, V.K., Tonle, I.K., Tertis, M.C., Ngameni, E., Jitaru, M., 2010. Adsorption of 2,4-dinitrophenol and 2,6-dinitrophenol onto organoclays and inorganic–organic pillared clays. Environmental Engineering and Management Journal 9, 953–960.
Tombácz, E., Szekeres, M., 2004. Colloidal behavior of aqueous montmorillonite suspensions: the specific role of pH in the presence of indifferent electrolytes. Applied Clay Science 27, 75–94.
Tombácz, E., Csanaky, C., Illés, E., 2001. Polydisperse fractal aggregate formation in clay and iron oxide suspensions, pH and ionic strength dependence. Colloid & Polymer Science 279, 484–492.
Torres Sánchez, R.M., Falasca, S., 1997. Specific surface and surface charges of some Argentinean soils. Zeitschrift fur Pflanzenernahrung und Bodenkunde 160, 223–226.
Torres Sánchez, R.M., Genet, M.J., Gaigneaux, E.M., dos Santos Afonso, M., Yunes, S., 2011. Benzimidazole adsorption on the external and interlayer surfaces of raw and treated montmorillonite. Applied Clay Science 53, 366–373.
Yapar, S., Torres Sánchez, R.M., Emreol, M., Weidler, P., Emmerich, K., 2009. Microwave irradiation used for all steps of pre-pillaring Al-montmorillonite. Clay Minerals 44, 161–172.
Yuan, P., He, H., Bergaya, F., Wu, D., Zhou, Q., Zhu, J., 2006. Synthesis and characterization of delaminated iron-pillared clay with meso–microporous structure. Microporous and Mesoporous Materials 88, 8–15.
Yuan, P., Annabi-Bergaya, F., Taoa, Q., Fan, M., Liu, Z., Zhu, J., He, H., Chen, T., 2008. A combined study by XRD, FTIR, TG and HRTEM on the structure of delaminated Fe-intercalated/pillared clay. Journal of Colloid and Interface Science 324, 142–149.
Zhang, R., Krzyszowska-Waitkus, A., Vance, G., Qi, J., 2000. Pesticide transport in field soils. Advances in Environmental Research 4, 59–68.
Zermane, F., Bouras, O., Baudu, M., Basly, J.-P., 2010. Cooperative coadsorption of 4-nitrophenol and basic yellow 28 dye onto an iron organo–inorgano pillared montmorillonite clay. Journal of Colloid and Interface Science 350 (1), 315–319.
Zuo, S., Zhou, R., Qi, C., 2011. Synthesis and characterization of aluminum and Al/REE pillared clays and supported palladium catalysts for benzene oxidation. Journal of Rare Earths 29 (1), 52–57.